Leadership in Sustainable Infrastructure
Leadership en Infrastructures Durables

Vancouver, Canada
May 31 – June 3, 2017/ *Mai 31 – Juin 3, 2017*

A NOVEL APPROACH FOR STRESS-STRAIN CHARACTERIZATION OF METALLIC MATERIALS USING THE PRODUCT-LOG (OMEGA) FUNCTION

Ndubuaku, Onyekachi[1,6], Martens, Michael[2], Ahmed, Arman[3], Cheng, Roger[4] and Adeeb, Samer[5]

[1,3,4,5] University of Alberta, Canada
[2] TransCanada Pipelines Ltd., Canada
[6] ndubuaku@ualberta.ca

Abstract: The true stress-true strain characterization of a metallic material may be established using a constitutive mathematical expression such as the Ramberg-Osgood stress-strain equation, or any of the various alternative stress-strain curve models which have been developed for the characterization of metallic materials over the full-range of the stress-strain relationship. Some common drawbacks of the existing models have however been observed as most of the earlier and simpler models tend to lose their predictive accuracy beyond a limited strain range whereas, as the precision of the models is improved, significant complexity is usually introduced in the later and more accurate models due to a requirement for an increased number of constitutive parameters. This paper therefore presents a relatively simple stress-strain curve model which is proven to be easily applicable, and capable of accurate predictions over the full range of strains. The proposed stress-strain model is defined using only two model parameters and unlike many existing stress-strain models, can be easily applied to materials with a well-defined yield plateau. To evaluate the applicability of the proposed model, curve-fitting techniques are employed for comparison to experimental stress-strain data obtained from cryogenic tensile tests of three different metallic materials; 300 series austenitic stainless steel (AISI 304L), 5000 (Al–Mg) series aluminum alloy (AA5083), and nickel steel alloy (Invar steel-FeNi36). Using the proposed model, excellent approximations of the nonlinear load-deformation behavior of the tested specimens are observed over the full-range of the true stress-true strain relationship.

1 Introduction

With the development and application of various microstructure-transformation techniques, attempts have been made over the years to improve the ductility, strength properties, and strength-to-weight ratio characteristics of metallic materials. The chemical composition and thermo-mechanical processing route, which are the most influential factors of the resulting microstructure of metals, are invariably considered in the material selection process; which involves the determination of the appropriate combination of desired mechanical properties (strength, hardness, toughness, ductility, fatigue resistance, etc.) and non-mechanical properties (formability, wear resistance, corrosion resistance, machinability, weldability, etc.) for each specific civil engineering application (Kurzydłowski 1999).

Steels and cast irons are the most commonly used materials for the design and construction of civil engineering structures and their microstructural constituents (austenite, bainite, cementite, ferrite, martensite, and pearlite), as well as the multiphase character of their microstructure can be systematically manipulated or altered to yield desired performances for various structural applications (Davis 1998). According to Zhao et al. (2014), the Transformation Induced Plasticity (TRIP) concept has been used in

automotive applications for many years and has recently begun to receive much attention due to excellent improvements obtained in the outstanding combination of ductility and strength of steels. TRIP techniques include processes such as intercritical annealing (IA), severe plastic deformation (SPD), quenching and partitioning traeatment (Q&P), accumulative roll bonding (ARB), bimodal grain size distribution, etc. (Valiev et al. 1993, Jacques 2004, Bouquerel et al. 2006, Terada et al. 2007, Shen et al. 2011, Bagliani et al. 2013).

A good illustration of the effect of thermo-mechanical processes on the mechanical behavior of metallic materials is given by Curtze et al. (2009) in their study on the dependence of the mechanical behavior of Dual Phase (DP) steels and TRIP steels on temperature and strain rate: while both DP and TRIP steels comprise multiphase microstructures, DP steels are obtained by intercritical annealing followed by quenching to room temperature in order to transform the ferrite/austenitic microstructure to martensite, while TRIP steels are obtained by inducing an isothermal hold below the bainite start temperature during cooling from the intercritical annealing temperature. Consequently, DP steels typically possess a two-phase ferritic-martensitic microstructure whereas the microstructure of TRIP steels is characterized by an embedment of bainite, martensite, and retained autensite in a continuous ferrite matrix. They explain that the soft ferritic phase associated with DP and TRIP steels is the main factor responsible for their characteristic low yield strengths whereas the hard martensite and bainite constituents dispersed in the ferrite matrix are responsible for high ultimate strength and strain-hardenability.

Thermo-mechanical loading in the operational phase of a material's lifecycle also affects the deformability of polycrystalline materials such as metals and metallic alloys, and is a direct consequence of microstructural gliding dislocation and grain boundary characteristics. Therefore, under subjection to loading, the mechanical behavior of metallic materials is significantly affected by temperature and strain rate: the effect of thermal energy makes it easier for gliding dislocations to occur thereby decreasing the strength with increasing temperature and, on the other hand, development of various interfacial slip-resisting mechanisms cause an increase of the strength with increasing strain rate (Slavik and Sehitoglu 1986, Davis 1998).

The mechanical behavior of metallic materials is generally characterized by a nonlinear stress-strain relationship typically obtained from the results of an axial tension coupon test carried out in a laboratory-controlled environment. Due to the nonlinearity associated with the load-deformation characteristics of metallic materials, an appropriate mathematical expression, comprising a number of defining constituent parameters, is usually employed for describing a reasonable approximation of the stress-strain relationship. With the modern-day existence of fast and efficient computational capability, simulation of the mechanical behavior of materials used in the design and construction of civil engineering structures, and under subjection to several loading configurations, is easily achieved using a variety of numerical evaluation tools. To ensure the accuracy of computational simulations, it is however imperative that the constitutive equation used to describe the mechanical behavior of materials is robust and precise.

The Ramberg-Osgood equation (ROE), which expresses the strain as a function of the stress and is governed by two material constants (the 0.2% proof stress $\sigma_{0.2}$ and the initial elastic modulus E_o) and one model constant (the strain-hardening exponent, n), has been widely-adopted for many civil engineering applications but has also been observed to be incapable of providing excellent approximations of material stress-strain behavior beyond the 0.2% proof stress. In a bid to improve the predictive accuracy of the ROE, a number of modified stress-strain expressions have been subsequently put forward by several researchers. Most of the modified expressions are however designed to capture the tensile stress-strain behavior of metallic materials at room temperature. (Ramberg and Osgood 1943, Skelton et al. 1997, Macdonald et al. 2000, Mirambell and Real 2000, Chryssanthopoulos and Low 2001, Gardner and Nethercot, 2004).

After exposure to either cryogenic or elevated temperatures, significant alterations occur to the mechanical behavior of metallic materials and past research has indicated that the behavior of structures is usually very complex either when using precooled or preheated materials or when using materials in environments with temperatures significantly above or below ambient temperature. The load-deformation characteristics of structural elements and components have been determined to be highly sensitive to the stress-condition relative to the affected mechanical properties. A few researches have been carried out to study the effects

of high and low temperatures on the stress-strain behavior of various metallic materials and a number of constitutive stress-strain equations have been developed for structural analysis and design purposes (Buchanan et al. 2004, Chen and Young 2006, Park et al. 2011, Yoo et al. 2011, Wang et al. 2014).

It is generally desirable that the mathematical expressions used to describe the stress-strain behavior of metallic materials are versatile enough such that the model parameters can be easily adjusted to define the changes in the stress-strain curve due to temperature- and strain rate-induced microstructural alterations. However, there are some important limitations associated with existing stress-strain models: the simpler models lack the desired robustness and accuracy for defining a wide range of stress-strain behaviors, and the applicability of more advanced models is hampered by the large number of constituent parameters required for improved accuracy. A novel stress-strain curve model that is capable of providing an accurate approximation of the stress-strain behavior of metallic materials at different temperatures and strain rates, is presented in this paper. The practicality and efficiency of the proposed model is illustrated by comparison of model-approximated stress-strain curves (derived using the proposed equation) to experimental stress-strain curves obtained from previous research by Park et al. (2011) on the cryogenic tensile behavior of three different materials over a range of temperatures and strain rates, and excellent correlations are observed for all the comparisons.

2 Background

A typical stress-strain curve is plotted using the stress and strain values obtained from a standard uniaxial tensile test of a material specimen. The nominal stress values are established using the original cross-section area of the specimen while the nominal strain values are determined as the average strain over the originally specified gauge length. The nominal (or so-called “engineering”) stress and strain values obtained directly from the coupon test experiments do not portray a realistic representation of the load-deformation process, especially at high levels of axial deformation, due to non-consideration of the simultaneous changes in geometric dimensions alongside axial deformation and development of non-uniform stress-strain distributions (Adeeb, 2011). For practical applications, it is therefore preferable to determine the true stress-true strain relationship from the tensile test based on instantaneous values of the geometric dimensions of the material specimen and gauge length (Mackenzie 1997, Arasaratnam et al. 2011).

3 Review of existing stress-strain equations

The power-law approach provides a feasible option for mathematical representation of the nonlinearity associated with the stress-strain behavior of metallic materials hence many of the earliest stress-strain curve equations, as well as the subsequent modifications, are essentially based on an expression of the stress as a power function of the strain or vice versa (Ludwik 1909, Ramberg and Osgood 1943, Hollomon 1945). The ROE expresses the strain as a function of the stress based on the following equation:

$$[1] \quad \varepsilon = \frac{\sigma}{E_o} + \varepsilon_{0.2}\left(\frac{\sigma}{\sigma_{0.2}}\right)^{n_{RO}}$$

where σ represents the true stress and ε represents the true strain. $\sigma_{0.2}$ represents the 0.2% proof stress and E_o represents the initial elastic modulus. The strain parameter, $\varepsilon_{0.2}$, is generally determined as the value of the plastic strain corresponding to the *offset yield strength,* $\sigma_{0.2}$ (taken as 0.002), and n_{RO} represents the strain-hardening component, given by:

$$[2] \quad n_{RO} = \frac{In(20)}{In(\sigma_{0.2}/\sigma_{0.01})}$$

A slightly-modified version of the ROE is expressed by API 579-1/ASME FFS-1 (2007) as follows:

$$[3] \quad \varepsilon = \frac{\sigma}{E_o} + \left(\frac{\sigma}{H_{RO}}\right)^{\frac{1}{n_{RO}}}$$

Where multiple data points for a stress-strain curve are provided, the constants (H_{RO} and n_{RO}) are derived using curve-fitting regression techniques otherwise, where only the yield strength (σ_y) and ultimate tensile strength (σ_u) are known, the constants are obtained (for the range $0.02 \leq \sigma_y/\sigma_u \leq 1.0$) as follows:

$$[4] \quad n_{RO} = \frac{1 + 1.3495\left(\frac{\sigma_y}{\sigma_u}\right) - 5.3117\left(\frac{\sigma_y}{\sigma_u}\right)^2 + 2.9643\left(\frac{\sigma_y}{\sigma_u}\right)^3}{1.1249 + 11.0097\left(\frac{\sigma_y}{\sigma_u}\right) - 11.7464\left(\frac{\sigma_y}{\sigma_u}\right)^2}$$

$$[5] \quad H_{RO} = \frac{\sigma_u \, exp[n_{RO}]}{{n_{RO}}^{n_{RO}}}$$

Mirambell and Real (2000) proposed a modification of the ROE to improve the approximation of the stress-strain curve beyond the 0.2% proof stress. The modified formula was obtained by applying a linear transformation of the stress and strain axes origin to the 0.2% proof stress point of the curve, and then using the ROE in the new reference system. Rasmussen (2003) modified the Mirambell-Real expression by replacing the ultimate plastic strain ($\varepsilon_{p,u}$) by the total ultimate strain (ε_u) and developed the equations for the second-stage strain-hardening exponent, *m,* the total ultimate strain, ε_u, and the ultimate strength, σ_u, using the three basic ROE parameters.

The two-stage approach proposed by Mirambell and Real (2000) and Rasmussen (2003) was extended by Chen and Young (2006) to the stress-strain characterization of stainless steel types EN 1.4462 (Duplex) and EN 1.4301 (AISI 304) at temperatures ranging from 20^{0}C to 1000^{0}C:

$$[6] \quad \varepsilon_T = \begin{cases} \frac{f_T}{E_{0,T}} + 0.002\left(\frac{f_T}{f_{y,T}}\right)^{n_T} & for\ f_T \leq f_{y,T} \\ \frac{f_T - f_{y,T}}{E_{y,T}} + \varepsilon_{u,T}\left(\frac{f_T - f_{y,T}}{f_{u,T} - f_{y,T}}\right)^{m_T} + \varepsilon_{y,T} & for\ f_T > f_{y,T} \end{cases}$$

where f_T, $f_{u,T}$, and $f_{y,T}$ represent the stress, the ultimate stress, and the 0.2% proof stress at the temperature *T (*in ^{0}C) respectively. ε_T, $\varepsilon_{u,T}$, and $\varepsilon_{y,T}$ represent the strain, the strain corresponding to ultimate stress, and the strain corresponding to proof stress at the temperature *T (*in ^{0}C) respectively. $E_{0,T}$ is the initial elastic modulus at the respective temperature *T (*in ^{0}C) and the tangent modulus of the temperature-altered stress-strain curve at the 0.2% proof stress, $E_{y,T}$ is derived as:

$$[7] \quad E_{y,T} = \frac{E_{0,T}}{1+0.002\, n_T \frac{E_{0,T}}{f_{y,T}}}$$

and the first-stage strain-hardening exponent, n_T and the second-stage strain-hardening exponent, m_T are both derived as:

$$[8] \quad n_T = 6 + 0.2\sqrt{T}$$

$$[9] \quad m_T = \begin{cases} 5.6 - \frac{T}{200} & (for\ stainless\ steel\ type\ EN\ 1.4462) \\ 2.3 - \frac{T}{200} & (for\ stainless\ steel\ type\ EN\ 1.4462) \end{cases}$$

Chen and Young determined that the temperature-altered material properties (the 0.2% proof stress, $f_{y,T}$; the initial elastic modulus, $E_{0,T}$; the ultimate stress, $f_{u,T}$; and the ultimate strain, $\varepsilon_{u,T}$) can be expressed as the following function of the temperature:

$$[10] \quad \frac{P_T}{P_N} = A_T - \frac{(T - B_T)^{D_T}}{C_T}$$

where P_N and P_T represent the value of any of the four above-listed material properties at the normal room temperature and the temperature-altered value respectively, and the coefficients A_T, B_T, C_T and D_T are empirically obtained from the results of the experiment.

Based on the constitutive model (BP model) developed by Bodner and Partom (1975) for representing time-dependent phenomena such as viscoplasticity and inelastic creep behavior, Park et al. (2011) studied the effect of temperature and strain rate on - and proposed a unified constitutive equation for - the nonlinear material behavior of AISI 300 series ASS, aluminium alloy, and nickel steel alloys. To account for the effect of microstructural phase transformation on the plastic deformation characteristics of the material, the strain-hardening rate and the strain-rate sensitivity are directly used as the material parameters. The BP model does not explicitly incorporate the yield function but is observed to be capable of expressing the yield phenomenon of materials (Yoo et al. 2011).

The BP model expresses the total strain rate, $\dot{\varepsilon}_{ij}$, as a sum of the elastic strain rate, $\dot{\varepsilon}^e_{ij}$, and the inelastic strain rate, $\dot{\varepsilon}^p_{ij}$:

$$[11] \quad \dot{\varepsilon}^p_{ij} = D_o exp\left\{-\frac{1}{2}\left(\frac{Z}{\sigma_{eff}}\right)^{2N}\right\}\frac{\sqrt{3}S_{ij}}{\sigma_{eff}}$$

where σ_{eff} and S_{ij} represent the effective stress and the deviatoric stress respectively. D_o, N and Z are the internal parameters: D_o sets the maximum limit for the strain rate predicted by the model and N controls the strain rate sensitivity. The strain-hardening behavior of the material is controlled by Z which is derived, for the case of isotropic hardening, as:

$$[12] \quad Z = Z_1 + (Z_0 - Z_1).exp\left(-mW_p\right)$$

Z_0, Z_1, and m control the yield stress, saturation of stress, and the slope of the hardening curve respectively. The plastic work, W_p is derived as:

$$[13] \quad W_p = \int dW_p = \int \sigma_{ij} d\varepsilon^p_{ij}$$

One of the most recent and versatile stress-strain models, developed by Zhang and Alam (2017), was specifically proposed to describe the stress-strain behavior of steel sheet materials that exhibit a relatively long yield plateau. The Zhang-Alam model is an expanded Ramberg-Osgood model expressed as:

$$[14] \quad \varepsilon = \begin{cases} {\sigma}/{E} & 0 \le \sigma \le \sigma_e \\ {\sigma}/{E} + k_1\left({\sigma}/{E}\right)^{n_1} & \sigma_e < \sigma \le f_y \\ \varepsilon_y + {\left(\sigma - f_y\right)}/{\alpha E} & f_y < \sigma \le \sigma_p \\ {\sigma}/{E} + k_2\left({\sigma}/{E}\right)^{n_2} & \sigma > \sigma_p \end{cases}$$

where σ, ε and E represent the true stress, true strain, and the Young's modulus respectively. f_y represents the lower yield strength and ε_y represents the strain at f_y. σ_e is the proportional limit; described by the point where the relative difference between the R-O stress and the linear stress is larger than 0% but less than or equal to 0.5%. α is a coefficient multiplied with E which represents the slope of the yielding platform. ε_p represents the strain at the intersection of a yielding platform and initial strain hardening portion. n_1, n_2, k_1, and k_2 are the model constants derived by equations described in Zhang and Alam (2017).

The Mirambell-Real and Rasmussen models adopted by Chen and Young for material characterization at elevated temperatures and the modifications applied to the BP model by Park et al. exhibit advanced capabilities for stress-strain curve approximation over the full range of strains for a wide range of

applications. Zhang and Alam's expanded R-O model was also observed to perform well in approximating the stress-strain curve of steel sheet materials with well-defined yield plateau; with errors beyond the proportional limit < 5%. However, as is observable from the above-presented expressions, the applicability of the proposed models is limited by the associated complexity and numerous constituent parameters. The proposed stress-strain curve model presented in this study provides a simpler and equally accurate alternative to existing models and is shown to be capable of providing a reasonable approximation of the yield plateau in materials that exhibit a well-defined yield point. The motivation for the proposed model in this study is the development of a stress-strain curve model which is capable of providing a reasonable approximation of both continuous hardening-type stress-strain curves and yield plateau-type stress-strain curves.

4 Description of the proposed stress-strain curve model

The novel stress-strain curve model presented in this paper is herein referred to as the 'Ndubuaku model'. The proposed equation is initially derived by expressing the stress as a function of the strain using a power-law function and subsequently, an explicit inverted expression of the strain as a function of the stress is derived based on the product log (omega) function:

$$[14] \quad \sigma_R = \varepsilon_R^{\frac{-\left(\frac{1}{H_{NM}}\right)}{K_{NM}}}$$

σ_R is the stress ratio, derived as the ratio of the true stress σ to the full stress range (i.e., the difference between the ultimate stress, σ_u, and the proportionality limit stress, σ_{pl}), and is expressed as:

$$[15] \quad \sigma_R = \frac{\sigma}{\left(\sigma_u - \sigma_{pl}\right)}$$

ε_R is the strain ratio, derived as the ratio of the true strain ε to the full strain range (i.e., the difference between the ultimate strain, ε_u, and the corresponding total strain at the proportionality limit stress, ε_{pl}), and is expressed as:

$$[16] \quad \varepsilon_R = \frac{\varepsilon}{\left(\varepsilon_u - \varepsilon_{pl}\right)}$$

K_{NM} and H_{NM} are the model parameters, empirically derived from the material test, and are herein referred to as the 'knee' parameter and the 'heel' parameter respectively. The model parameters both control the strain-hardening behavior of the stress-strain curve. However, the 'knee' parameter, K_{NM} has a more noticeable effect on the convexity of the upper portion of the stress-strain curve whereas the effect of the 'heel' parameter, H_{NM} is more significant on the concavity of the lower portion of the curve.

The *Product log* function is expressed in the following form:

$$y = xe^x \Leftrightarrow W(y) = x$$

Hence, the inverted closed-form expression of the strain as a function of the stress is expressed as:

$$[17] \quad \varepsilon_R = e^{-H_{NM} \cdot \mathrm{W}\left[-\frac{K_{NM}}{H_{NM}} \cdot In(\sigma_R)\right]}$$

5 Evaluation of model applicability

Park et al. (2011) explained that the 300 series of austenitic stainless steel (ASS), aluminum alloys, and nickel steel provide high strength and excellent ductility over a wide range of low temperatures hence, they are generally preferred over other metallic materials for cryogenic applications in many industrial fields. In an effort to introduce a robust design scheme for structures used for storing and shipping liquefied natural gas (LNG), they conducted a series of cryogenic tensile tests under various temperatures (110 - 293 K) and strain rates (0.00016 - 0.01 s^{-1}). The material specimens for the tests were obtained from the three representative types of low-temperature application materials; AISI 304L, AA5083, and Invar steel.

To properly portray the robustness and versatility of the proposed model, the results of the cryogenic tensile tests conducted by Park et al. have been selected for model evaluation. The test matrix for the experiments was designed such that five graduations of temperature (293K, 223K, 153K, 133K, and 110K) were selected, and three strain rates ($0.00016s^{-1}$, $0.001s^{-1}$, $0.01s^{-1}$) were determined as the test variables at each temperature; however, only two arrays of results from the test matrix was utilized for the model evaluation.

The stress-strain data obtained from the results of the experimental studies conducted by Park et al. were converted to the respective true stress and true strain values. However, the portion of the stress-strain curve beyond the ultimate stress (after the onset of necking) was excluded from the model evaluation as it is considered to be practically irrelevant to the applicability of the proposed model. The ultimate stresses (σ_u) used for the model evaluation were taken as the highest values of true stress reported from the experiments, while the ultimate strains (ε_u) were taken as the corresponding values of true strain at the respective ultimate stresses.

The proposed model is applied to the stress-strain curve in two segments: the linear elastic portion of the curve is defined by the initial modulus of elasticity of the material, E_o, up to the proportionality limit stress and from the proportionality limit, the nonlinear stress-strain relationship is defined using the proposed expression up to the ultimate limit. Least-squares curve fitting was used to obtain the best fit between the experimental data points and the model-predicted stress-strain curve by minimizing the sum of the squares of the errors between the model-predicted values and the experimentally-obtained values for each data point. The plots of the model-to-experiment curve-fit evaluations are presented in Figures 2 to 7.

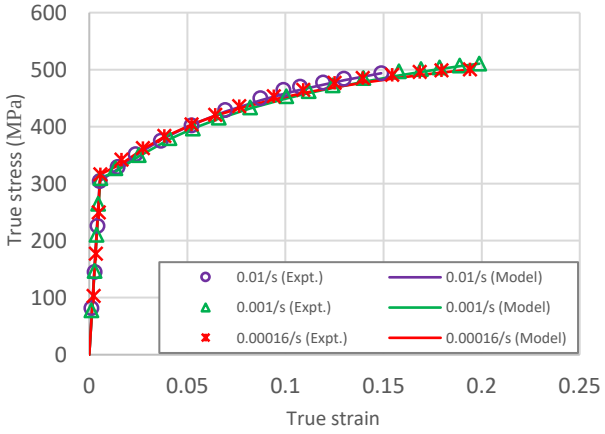

Figure 2: Model-to-experiment stress-strain plots for AA5083 at 110K (strain rate - varied)

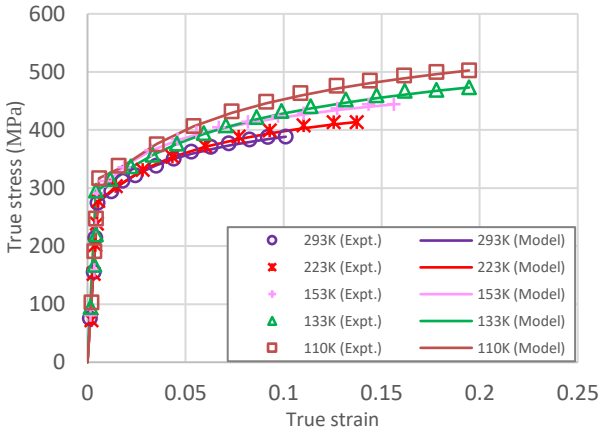

Figure 3: Model-to-experiment stress-strain plots for AA5083 at 0.00016/s (temperature - varied)

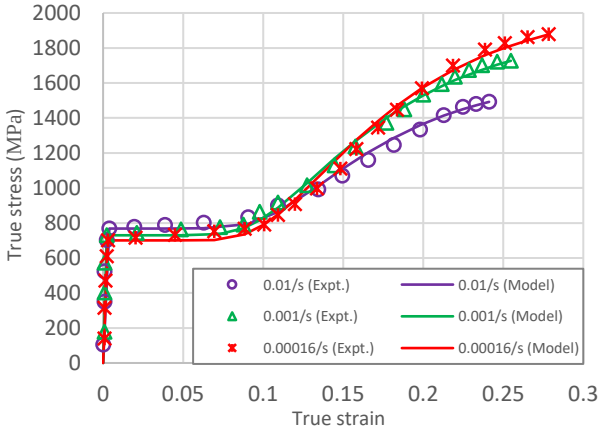

Figure 4: Model-to-experiment stress-strain plots for AISI 304L at 110K (strain rate - varied)

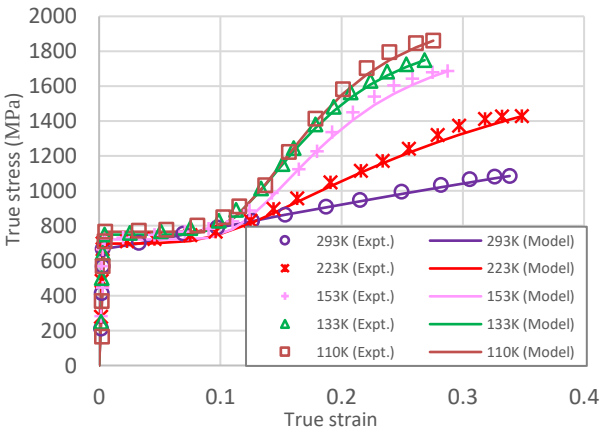

Figure 5: Model-to-experiment stress-strain plots for AISI 304L at 0.00016/s (temperature - varied)

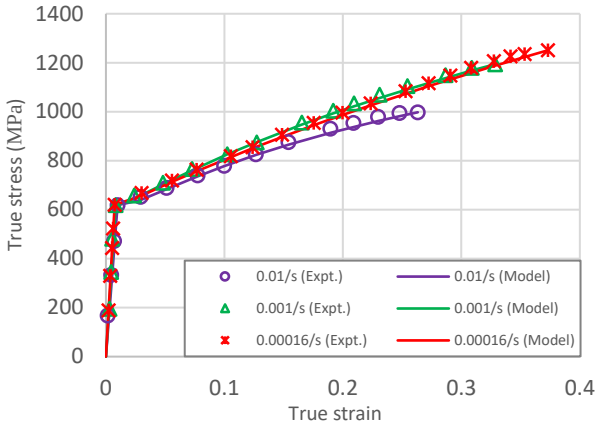

Figure 6: Model-to-experiment stress-strain plots for Invar Steel at 110K (strain rate - varied)

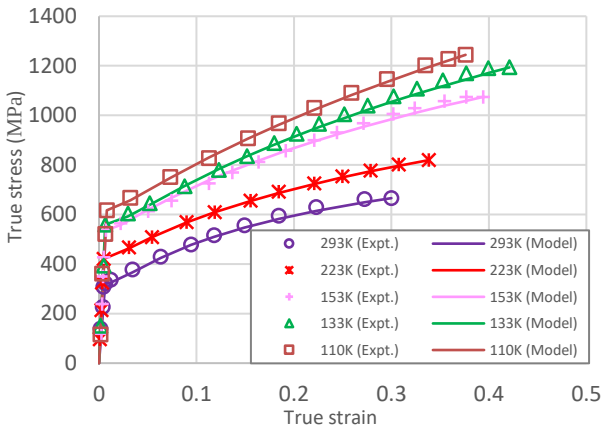

Figure 7: Model-to-experiment stress-strain plots for Invar Steel at 0.00016/s (temperature - varied)

The R-squared values and values of the model parameters are presented for the strain rate-effect tensile tests and the temperature-effect tensile tests in Table 1.

Table 1: Model parameters and R^2 values for model-to-experiment curve-fit evaluations

Material	Model parameters	Strain rate (sec^{-1})			Temperature (K)				
		0.01	**0.001**	**0.00016**	**293**	**223**	**153**	**133**	**110**
AA 5083	K_{NM}	2.17	2.31	2.79	2.71	2.89	3.25	2.78	2.71
	H_{NM}	4.92	4.49	3.55	4.26	4.09	4.91	4.24	3.64
	R^2	0.9986	0.9988	0.9981	0.9976	0.9984	0.9986	0.9987	0.9989
AISI 304L	K_{NM}	1.32	1.56	1.74	1.12	1.52	1.53	1.66	1.71
	H_{NM}	0.68	0.71	0.73	13.53	0.98	0.67	0.62	0.59
	R^2	0.9924	0.9962	0.9939	0.9989	0.9961	0.9973	0.9989	0.9985
Invar Steel	K_{NM}	1.46	1.38	1.25	2.03	1.68	1.58	1.46	1.34
	H_{NM}	5.12	8.69	12.52	4.02	6.73	7.06	7.17	8.95
	R^2	0.9981	0.9993	0.9994	0.9982	0.9998	0.9979	0.9988	0.9996

The high R-squared values presented in Table 1, as obtained from the curve-fit evaluations in Figures 2 to 7, indicate that the proposed model provides a highly accurate approximation of the stress-strain curves for all the experimental results considered.

From the observed consistency in the variation of the obtained results, it is evident that the range of the values of the model parameters are reflective of the shape of the stress-strain curve. An explanation is given of the mean value and standard deviation of the model parameters, for a combination of the temperature- and strain rate-effect tensile tests of the three studied materials, as follows:

AA5083- The mean value and standard deviation of K_{NM} are 2.701 and 0.335 respectively, while the mean value and standard deviation of H_{NM} are 4.263 and 0.511 respectively. The mean value of H_{NM} is higher than the mean value of K_{NM}, indicating that the convexity of the 'knee' of the curve is favoured relative to the concavity of the 'heel'.

AISI304L- Considering the values obtained at 0.00016/s and 293K as outliers, the mean value and standard deviation of K_{NM} are 1.577 and 0.143 respectively, while the mean value and standard deviation of H_{NM} are 0.711 and 0.128 respectively. The mean value of H_{NM} is lower than the mean value of K_{NM}, indicating that the concavity of the 'heel' of the curve is favoured relative to the convexity of the 'knee'.

Invar Steel- The mean value and standard deviation of K_{NM} are 1.523 and 0.245 respectively, while the mean value and standard deviation of H_{NM} are 7.533 and 2.602 respectively. The mean value of H_{NM} is higher than the mean value of K_{NM}, indicating that the convexity of the 'knee' of the curve is favoured compared to the concavity of the 'heel'.

A comparison between the obtained results for AA5083 and Invar Steel indicates that when the value of K_{NM} is significantly reduced (approximately below a value of 2), the positive effect of a higher value of H_{NM} on the convexity of the knee begins to diminish infinitely. Also, a low value of H_{NM} (approximately below a value of 3) typically indicates the presence of a yield plateau in the stress-strain curve. However, the yield plateau diminishes as the ratio of K_{NM} to H_{NM} exceeds a value of 6. The knee-to-heel parameter ratio that causes the yield plateau to vanish reduces as the value of H_{NM} increases.

6 Conclusions

Complex nonlinearities and plasticization problems are frequently encountered in the design and analysis of civil engineering structures and structural elements. Past research studies indicate that the phase transformations that occur within the microstructure are the most important factors that cause significant changes in the mechanical behaviour of metallic materials; especially at varying temperatures and strain rates. Proper characterisation of the stress-strain behaviour of materials is therefore important for practical considerations, especially where parametric numerical simulations are required for structural design and analysis. A novel stress-strain curve model has been developed and presented in this paper to provide a simple and accurate tool for parameterization of the strength and strain-hardening characteristics of different structural materials, over a wide range of processing and operational conditions. The proposed model is established based on the true stress-true strain relationship and only requires empirical derivation of two model parameters for the approximation of the stress-strain curve over the full range of strains; even for materials with a well-defined yield plateau. The most important characteristic of the proposed model is the ability to describe a continuous transition from yield plateau-type stress-strain curves to continuous hardening-type stress-strain curves; even so that curves that may be regarded as bilinear (as in Figure 6) can also be approximated. The robustness and precision provided by the proposed model are illustrated by the model-to-experiment curve-fit evaluations presented in this paper.

References

Adeeb, S.M., 2011. *Introduction to solid mechanics and finite element analysis using Mathematica*. Dubuque, IA: Kendall Hunt Publishing Company.

Arasaratnam, P., Sivakumaran, K.S. and Tait, M.J., 2011. True stress-true strain models for structural steel elements. *ISRN Civil Engineering*, *2011*.

Bagliani, E.P., Santofimia, M.J., Zhao, L., Sietsma, J. and Anelli, E., 2013. Microstructure, tensile and toughness properties after quenching and partitioning treatments of a medium-carbon steel. *Materials Science and Engineering: A*, **559**: 486-495.

Bodner, S. and Partom, Y., 1975. Constitutive equations for elastic-viscoplastic strain-hardening materials. *Journal of Applied Mechanics*, **42**(2): 385-389.

Bouquerel, J., Verbeken, K. and De Cooman, B.C., 2006. Microstructure-based model for the static mechanical behaviour of multiphase steels. *Acta Materialia*, **54**(6): 1443-1456.

Buchanan, A., Moss, P., Seputro, J. and Welsh, R., 2004. The effect of stress–strain relationships on the fire performance of steel beams. *Engineering Structures*, **26**(11): 1505-1515.

Chen, J. and Young, B., 2006. Stress–strain curves for stainless steel at elevated temperatures. *Engineering Structures*, **28**(2): 229-239.

Chryssanthopoulos, M.K. and Low, Y.M., 2001. A method for predicting the flexural response of tubular members with non-linear stress–strain characteristics. *Journal of Constructional Steel Research*, **57**(11): 1197-1216.

Curtze, S., Kuokkala, V.T., Hokka, M. and Peura, P., 2009. Deformation behavior of TRIP and DP steels in tension at different temperatures over a wide range of strain rates. *Materials Science and Engineering: A*, **507**(1): 124-131.

Davis, J.R., 1998. Metals Handbook: Desk Edition 2nd edn. Materials Park, OH: ASM International.

Gardner, L., and Nethercot, D. A. (2004a). Experiments on stainless steel hollow sections. Part 1: Material and cross-sectional behavior. *Journal of Constructional Steel Research*, **60**: 1291–1318.

Hollomon, J. H., 1945. Tensile Deformation. *Transactions of the Metallurgical Society of AIME*. **162**: 268-290.

Jacques, P.J., 2004. Transformation-induced plasticity for high strength formable steels. *Current Opinion in Solid State and Materials Science*, **8**(3): 259-265.

Kurzydłowski, K.J., 1999. Structure and properties of metals. *Acta Physica Polonica A*, **96**(1): 69-79.

Ludwik, P., 1909. *Elemente der Technologischen Mechanik*. Berlin: Verl. v. Julius Springer.

Macdonald, M., Rhodes, J., and Taylor, G. T., 2000. Mechanical properties of stainless steel lipped channels. *Proc., 15th Int. Specialty Conference on Cold-Formed Steel Structures*, University of Missouri-Rolla, Mo., 673–686.

Mackenzie, A.C., Hancock, J.W. and Brown, D.K., 1977. On the influence of state of stress on ductile failure initiation in high strength steels. *Engineering fracture mechanics*, **9**(1): 167IN13169-168IN14188.

Mirambell, E. and Real, E., 2000. On the calculation of deflections in structural stainless steel beams: an experimental and numerical investigation. *Journal of Constructional Steel Research*, **54**: 109-133.

Mohammad, Z.H., Nouri, E., Khedmati, M.R., and Roshanali, M.M., 2010. Degradation of the compressive strength of unstiffened/stiffened steel plates due to both-sides randomly distributed corrosion wastage. *Latin American Journal of Solids and Structures*, **7**(3): 335-367.

Park, W.S., Chun, M.S., Han, M.S., Kim, M.H. and Lee, J.M., 2011. Comparative study on mechanical behavior of low temperature application materials for ships and offshore structures: Part I—Experimental investigations. *Materials Science and Engineering: A*, **528**(18): 5790-5803.

Park, W.S., Lee, C.S., Chun, M.S., Kim, M.H. and Lee, J.M., 2011. Comparative study on mechanical behavior of low temperature application materials for ships and offshore structures: Part II–Constitutive model. *Materials Science and Engineering: A*, **528**(25): 7560-7569.

Ramberg, W. and Osgood, W. R., 1943. *Description of stress-strain curves by three parameters*. Technical Note No. 902. Washington, DC, USA: National Advisory Committee for Aeronautics.

Rasmussen, K. J. R. 2003. Full-range stress-strain curves for stainless steel alloys. *Journal of Constructional Steel Research*, **59**: 47–61.

Shen, Y.F., Wang, C.M. and Sun, X., 2011. A micro-alloyed ferritic steel strengthened by nanoscale precipitates. *Materials Science and Engineering: A*, **528**(28): 8150-8156.

Skelton, R.P., Maier, H.J. and Christ, H.J., 1997. The Bauschinger effect, Masing model and the Ramberg–Osgood relation for cyclic deformation in metals. *Materials Science and Engineering: A*, **238**(2): 377-390.

Slavik, D. and Sehitoglu, H., 1986. Constitutive models suitable for thermal loading. *Journal of Engineering Materials and Technology,* **108**: 303-312.

Terada, D., Inoue, S. and Tsuji, N., 2007. Microstructure and mechanical properties of commercial purity titanium severely deformed by ARB process. *Journal of Materials Science*, **42**(5): 1673-1681.

Valiev, R.Z., Korznikov, A.V. and Mulyukov, R.R., 1993. Structure and properties of ultrafine-grained materials produced by severe plastic deformation. *Materials Science and Engineering: A*, **168**(2): 141-148.

Wang, X.Q., Tao, Z., Song, T.Y. and Han, L.H., 2014. Stress–strain model of austenitic stainless steel after exposure to elevated temperatures. *Journal of Constructional Steel Research*, **99**: 129-139.

Yoo, S.W., Lee, C.S., Park, W.S., Kim, M.H. and Lee, J.M., 2011. Temperature and strain rate dependent constitutive model of TRIP steels for low-temperature applications. *Computational Materials Science*, **50**(7): 2014-2027

Zhang, P., and Alam, M. S., 2017. Experimental investigation and numerical simulation of pallet-rack stub columns under compression load. *Journal of Constructional Steel Research*, **133**: 282-299.

Zhao, X., Shen, Y., Qiu, L., Liu, Y., Sun, X. and Zuo, L., 2014. Effects of Intercritical Annealing Temperature on Mechanical Properties of Fe-7.9 Mn-0.14 Si-0.05 Al-0.07 C Steel. *Materials*, **7**(12): 7891-7906.